CR# 141480

Task III-Data Dump

15 November 1974

High Performance

N_2O_4/Amine Elements - "Blowapart"

Contract NAS 9-14186

Report 14186-DRL-3-1

Prepared By:
B. R. Lawver

Prepared For:

NASA-Johnson Space Center
Houston, Texas

(NASA-CR-141480) HIGH PERFORMANCE N2O4/AMINE ELEMENTS: BLOWAPART (Aerojet Liquid Rocket Co.) 43 p HC $3.75 CSCL 21I

N75-30326

G3/28

Unclas
33801

Aerojet Liquid Rocket Company

TABLE OF CONTENTS

FIGURE LIST

TABLE LIST

I INTRODUCTION AND SUMMARY

The objective of this program is to develop an understanding of the mechanisms controlling hypergolic propellant blowapart and with that understanding develop a model containing the parameters controlling blowapart which will aid the design of stable high performing injectors. The mechanisms will be defined through test and analysis of subscale injectors using principally N_2O_4/MMH propellants and injectors and test conditions representative of the OME and Space Tug applications.

The program consists of four tasks. The objectives of the Task I effort are; to critique all existing models relating to blowapart, to summarize and review all associated experimental data and formulate updated models. The Task II effort consist of preparing a detailed program plan. The objectives of the Task III effort are to define the mechanisms governing blowapart through the design, fab, test and analysis of single element injectors. The objectives of Task IV are to verify the mechanisms governing blowapart and to extend RSS mapping to other injector elements.

This document summarizes the work performed during the Task III effort. Results of the Task I model review effort indicated that neither of the two existing blowapart models (JPL model and ALRC model) adequately describes RSS nor correlates the experimental data. New data correlations were developed that show the parameters exhibiting a controlling influence over blowapart are the chamber pressure, orifice diameter, and propellant temperature. Four regimes of reactive impingement were defined:

- Mixing,
- Popping (cyclic blowapart),

- Low pressure separation ($P_c < 300$ psia)
- High pressure separation ($P_c \geq 300$ psia)

New model concepts of reactive impingement were formulated to account for all four modes. The high pressure mode of RSS was postulated to be caused by recirculation gas heating of the fuel s[illegible]m to its decomposition temperature ahead of impingement. However, subsequ[illegible]nt analytical calculations showed inadequate recirculation gas heating to cause RSS.

The objectives of Task III testing were to concentrate on the high pressure mode of RSS, to verify the model concepts, and to map regions of RSS for the unlike doublet injector element. High speed color movi[illegible] were used to verify operating modes. Tests with two unlike doublet elements of differing impingement lengths verify the high pressure model analytical results in that recirculation gas heating does not control RSS and that other mechanisms are operative.

Impingement point temperature measurements indicate the existence of two modes of high pressure RSS which are deper[illegible]ent [illegible] he pressure, temperature, and velocity. High speed color movies show that [illegible] degree of RSS increases gradually with increasing pressure and increasing fuel temperature.

II CONCLUSIONS

The conclusions drawn from the Task III testing are summarized in Table I.

III TEST RESULTS

The two unlike doublet injector elements shown in Figure 1, were tested over the range of parameters listed in Table II to determine their influence on RSS. The injector, test chamber, and test setup are described in detail in Section V.

The test objectives and results are summarized in Table III. A detailed test condition log was maintained and included as Table IV. The test data are stored in a computer data file for easy manipulation and correlation. A listing of the reduced data is shown in Table V.

The objectives of the first series of tests (#101-106) were to verify proper test stand operation and to check the photographic equipment. The tests showed that the backlighting intensity was too bright and that the test stand functioned as required. Examination of the movie pictures showed all of the tests to be separated. Separation is defined as the appearance of unmixed oxidizer in the spray field evidenced by clouds of dark brown NO_2. Although density gradients between the cold window purge gas and the hot combustion gas obscures detail in the impingement zone at the higher pressure, the spray field operating mode is readily discernible.

The backlight was modified prior to the next test series to improve photography. A sheet of polorized filter paper and a sheet of ground glass were placed between the Fresnel lense and the test chamber to reduce the backlighting intensity and to eliminate parallel light from the quartz lamp.

The next series of tests (#107-111) were run at lower pressures to determine the pressure limit of RSS. The onset of RSS was found to occur between 100 and 150 psia. The recirculation gas model developed in Task I had predicted separation at about 400 psia with MMH. RSS was found to gradually worsen with increasing pressure. The density gradients were still visible but their intensity was found to decrease with pressure. Good, clear pictures were obtained at the lower pressures (100-200 psi).

The next set of tests (#112-123) were run with A-50 to determine the influence of fuel vapor pressure on RSS. The hot gas recirculation model had predicted that A-50 would separate at 500 psia as compared to 400 psia for MMH. The data shows A-50 to separate at about 200 psia as compared to about 150 psia for the MMH. The increase in separation severity with pressure is readily apparent in Figure 2 which shows a series of single movie frames from successive tests at increasing chamber pressures. Test No. 117 was run at a lower injection velocity to determine its influence on RSS. The movie film shows notably less separation at the lower velocity (88 ft/sec) than at the nominal velocity (125 ft/sec). Subsequent temperature probing indicates the same trend.

The next series of tests (no. 124-132) were run with the short impingement length doublet to determine the influence on RSS. The Task I model had indicated that RSS should depend on impingement length. The movie data do not show any discernible difference in separation characteristics between the long impingement (0.160 in.) and the short impingement (0.060 in.) doublet elements.

Test Numbers 134-138 were run with heated fuel over the pressure range of 100-250 psia. The movies show a pronounced worsening of separation with increased fuel temperature. This influence is demonstrated by the movie frames shown in Figure 3. Also shown in Figure 3, is the thermocouple used to probe the impingement point in the subsequent set of tests. The onset of separation was found to occur at 100 psia with 200°F MMH.

The final test set (No. 139-152) were run with ambient temperature propellants and the thermocouple probe mounted as shown in Figure 3. Initially, a 0.010 in. dia thermocouple was used, however, it lacked sufficient mechanical strength to remain in a fixed position. It was discarded for a more rigid 0.020 in. dia thermocouple. The movies indicate some disruption of the impingement by the thermocouple particularly at the lower velocity conditions, however, the temperature data are reasonably consistent and orderly. The temperature probing technique appears to offer significant quantitative data and therefore will be improved for the Task IV testing.

The impingement point temperature was found to depend on the chamber pressure and the propellant velocity as shown in Figure 4. These influences appear to be accounted for by adding the propellant stream dynamic head to the chamber pressure as shown in Figure 5. Also included in Figure 5 are the saturation temperature lines for N_2O_4 and MMH. It appears that separation, as determined visually from the movies, occurs when the impingement point temperature exceeds the N_2O_4 saturation temperature and that there is a change in mode of separation when the temperature exceeds the MMH saturation temperature.

The impingement process was observed to be cyclic in nature in both the mixed and separated modes. The characteristic frequencies were the same in both modes, suggesting that it is characteristic of the ligament shedding process. Energetic cyclic blowapart (i.e., popping) was not observed on any of the tests. The Task I data correlations would indicate that none should occur over the range of variables tested.

IV MODEL CORRELATIONS

The RSS data for both MMH and A-50 fuels were plotted on the pressure versus temperature scales as shown in Figure 6 for comparison with the Task I data correlations. It is noted that the A-50 separates at a higher pressure than the MMH and that the pressure at which MMH separates decreases with increasing fuel temperature. The N_2H_4 data of Zung (Ref. 1) shown in Figure 7 does not reflect the influence of inlet temperature. Testing with N_2H_4 under similar conditions is recommended to confirm the differences.

Listed in Table VI are the predicted and measured RSS pressure limits for MMH and A-50 at ambient temperature. Also included is Zung's N_2H_4 data for reference. The pressure limits were predicted on the basis of the recirculation gas heating model developed in Task I. The model states that separation should occur at the pressure corresponding to the fuel vapor pressure at 450°F, the vapor phase decomposition temperature. It is seen that the pressure levels do not agree and that the trend in fuel type is correct for MMH and A-50 but not for N_2H_4. In view of this and the fact that the analytical calculations had indicated insufficient heating, the hot gas recirculation model does not appear valid.

The correspondence between heat release rates and the onset of RSS would seem to indicate a dependence on propellant reactivites as shown in Table VII.

The model concepts developed on Task I were based on the complex reaction mechanisms of hypergolic fuels. A summary of these concepts is included in Figure 8 for reference in discussing the temperature probe results. The temperature data of Figure 5 shows two modes of RSS as evidenced by a step change in temperature. The temperature discontinuity is indicative of a change in reaction mechanism as suggested by the popping regime mechanism (Figure 8). It is believed that low enthalpy surface reactions predominate at the lower pressure conditions. These reactions heat the propellants to their saturation temperatures and when the fuel saturation temperature is exceeded, the reaction switches to a high enthalpy gas phase reaction. The onset of visual separation occurs when the temperature exceeds the N_2O_4 saturation temperature.

A surface controlled reaction would be expected to be primarily a function of the propellant interfacial surface area which is expected to be related to propellant stream turbulence level or Reynold number. As shown in Figure 9 there is a dependence of ΔT_i on R_e up to the point of transition. A free jet may also experience some self atomization prior to impingement thus influencing effective surface area. The self atomization is characterized by the ratio of aerodynamic to surface tension forces as described by the Weber number. The impingement point temperature rise is plotted versus the fuel and the oxidizer Weber number in Figure 10. There appears to be some dependence of ΔT_i on Weber number. It is noted that the temperature transition occurs beyond the critical Weber No. which signifies the onset of self atomization and increased surface area.

On the basis of these results a model of surface controlled reactions is in the process of being developed but requires additional data which will be obtained during the Task IV testing. Computerized data correlations of all the Task I data will be developed on the basis of these model results.

V TEST HARDWARE AND SETUP

A. Test Apparatus

The test apparatus consists of a test chamber equipped with transparent viewing ports and removable injectors and nozzles as shown in Figure 11.

1. Test Chamber

The test chamber is machined from a 4-inch square x 6-inch long block of 304 CRES. The combustion chamber section is 4 inches long, to which a 2 in. L* spacer is bolted to increase the combustion zone length to 6 inches. The block is bored to provide a 2.75 inch diameter combustion chamber. Four circular quartz windows are provided to facilitate photography and to allow flexibility in photographic lighting of the combustion process. The windows are 1/2 inch thick to provide a safety margin for 1000 psia operation. The flat quartz windows are sandwiched between durabula gaskets for cushioning against ignition shocks and uneven loading. A silicon "O" ring provides sealing on the window periphery. Quartz provides good propellant compatibility and well defined optical properties.

An inert gas (GN_2) film purge is provided to prevent obscuring the view by propellant spray impingement on the windows. The gas purge flow is injected through four inlets into an annular manifold. The gas is directed from the manifold through an annular gap and made to flow around the periphery of the chamber wall. The gas passages are sized such that the GN_2 is injected into the chamber at 50 ft/sec at 300 psia chamber pressure to minimize mixing with the propellant spray and combustion gas.

Provision is made for mounting both high and low frequency response pressure transducers and thermocouples as required. The nozzles consist of removable copper inserts drilled to provide the desired operating pressures.

2. Injectors

The injector body is a cylindrical shaped "piston" designed to fit into the purge ring located at the forward end of the chamber. The injector is held in the purge ring by Allen head screws. A silicon rubber O-ring seals the injector to the purge ring.

The injector consists of a main body with brazed-on inlet tubes. Two injector patterns are incorporated in one body as shown in Figure 1 to reduce fabrication costs. The element design parameters are shown in Figure 1. The orifice L/D's are 24/1 with rounded inlets to provide controlled hydraulics. The injectors are made of 304 CRES to permit braze assembly and provide dimensionally stable orifices.

The injector orifices were flow tested prior to hot fire testing to verify impingement and pattern accuracy. The flow data are plotted in Figure 12.

A high frequency response Kistler pressure transducer mounting port was provided as shown in Figure 1 to measure impingement point disturbances.

B. Test Facility Setup

The test apparatus was setup in the Research Physics Laboratory Test Bay 2 shown in Figure 13.

A schematic of the propellant system used is shown in Figure 14. Propellant (MMH/A-50/NTO) is stored in 50-gallon, 3000-psi run vessels. Gaseous nitrogen pressurization of these systems was used to provide controlled run conditions over a wide range of injector and chamber pressures.

Propellant conditioning was provided by installing in-line heat exchangers immediately upstream of the thrust chamber valves. A hot water circulation type temperature conditioning system was used to provide independent conditioning of the ox and fuel to temperatures from ambient to 300°F.

A separately regulated GN_2 Supply was used to provide test chamber back pressure as well as provide window purge for the chamber view-ports.

C. Instrumentation

High speed color photographs of the spray field were taken with the photographic equipment shown in Figure 13. Pictures were taken at 8000 pictures per second (1.25 μ sec exposure) and at 400 PPS (25 μ sec exposure) with a Hycam Model 41-0004 high speed camera. Four hundred foot rolls of Ecktachrome EF No. 7242 film were used which allows approximately 0.6 sec. of constant speed frame rate at 8000 PPS and approximately 30 sec. constant speed @ 440 PPS.

Lighting of the spray field was accomplished with the use of three 1000-watt quartz iodine lamps focused with Fresnel lenses. One lamp was used to backlight the spray area with the second and third lamps used as top and front lighting to provide spray detail and definition.

High frequency and low frequency instrumentation listed in Tables VIII and IX were used in the locations shown in the schematic of Figure 15.

Low frequency response test parameters were recorded on a Consolidated Electrodynamics Corporation's direct writing oscillograph. The high frequency response data were recorded on a Sangamo Model 3564 analog tape recorder.

The operating point data indicated in Table IX were digitized and stored in the on-line HP 2100 A Computer/Real Time process controller for "quick look" test review.

REFERENCES

1. Zung, L. B., "Hypergolic Impingement Mechanisms and Criteria for Jet Mixing or Separation", presented at the 6th ICRPG Liquid Propellant Combustion Instability Conference, 9-11 September 1969

TABLE I

Task III - Definition Of Governing Mechanisms Conclusions

- RSS SEVERITY INCREASES WITH
  - PRESSURE
  - FUEL TEMPERATURE
  - PROPELLANT VELOCITY
- RSS DEPENDS ON FUEL
  - MMH > A-50
- RSS NOT DEPENDANT ON IMPINGEMENT LENGTH
  - RECIRCULATION GAS MODEL INVALID
- RSS OCCURS IN TWO MODES
  - LOW ENTHALPHY REACTION ($T_{f_{sat}} > T_i > T_{ox_{sat}}$)
  - HIGH ENTHALPHY REACTION ($T_i > T_{f_{sat}}$)

TABLE II

Task III - Definition Of Governing Mechanisms Test Variables

- PRESSURE
  - 100 - 1000 PSIA
- PROPELLANT TEMPERATURE
  - $70^{0}F$
  - $200^{0}F$
- VAPOR PRESSURE
  - A-50
  - MMH
- IMPINGEMENT LENGTH
  - 0.160 in.
  - 0.060 in.

TABLE III

Task III - Definition Of Governing Mechanisms Test Objectives & Results

TEST OBJECTIVE	FUEL	INJECTOR	T_O (°F)	T_F (°F)	P_C (PSIA)	NO. TESTS	RESULTS
CHECKOUT TESTS	MMH	LONG IMPING.	AMB	AMB	300-1000	6	ALL SHOWED SEP.
DETERMINE PRESSURE LIMIT FOR RSS	MMH	LONG IMPING.	AMB	AMB	100-300	5	SEP ABOVE 150 PSI
DETERMINE VAPOR PRESSURE EFFECT ON RSS	A-50	LONG IMPING.	AMB	AMB	100-1000	12	SEP ABOVE 200 PSI
DETERMINE EFFORT OF IMPING. LENGTH ON RSS	MMH	SHORT IMPING.	AMB	AMB	100-1000	9	NO DISCERNIBLE DIFFERENCE
DETERMINE EFFECT OF TEMPERATURE ON RSS	MMH	LONG IMPING.	AMB	200	100-250	5	SEP AT 100 PSI
MEASURE IMPINGEMENT POINT TEMPERATURE	MMH	LONG IMPING.	AMB	AMB	100-1000	14	IMPING. PT. TEMPERATURE IS VELOCITY & PRESSURE DEPENDANT

TABLE IV - TEST LOG

HIGH PERFORMANCE N_2O_4/AMINE ELEMENTS

TEST CONDITION LOG

Test No.	D_f	Fuel	P_c	MR	T_F	T_o	ΔP_f	Noz	P_{N2} (PSIG)	P_{OT} (PSIG)	P_{FT} (PSIG)	DATE	f-Stop	FR/Rate (PPS)	Process	Light Meter W/2 N.D.F.	Remarks
0C-27-101	.020	MMH	300	1.6	Amb	Amb	100	0.330	1350	385	385	10/1/74	16	400	Normal	18	Long Impingement Element
-102	.020	MMH	300	1.6	Amb	Amb	100	0.330	1350	380	390	10/1/74	11	400	Normal	18	Long Impingement Element
-103	.020	MMH	300	1.6	Amb	Amb	100	0.330	1350	385	385	10/1/74	22	400	Normal	18	Long Impingement Element
-104	.020	MMH	300	1.6	Amb	Amb	100	0.330	1350	385	385	10/1/74	3.3	8000	Normal	18	Long Impingement Element
-105	.020	MMH	500	1.6	Amb	Amb	100	0.265	1463	585	585	10/1/74	3.3	8000	1 Stop	18	Long Impingement Element
-106	.020	MMH	1000	1.6	Amb	Amb	100	0.187	1463	1085	1085	10/1/74	3.3	8000	Normal	18	Long Impingement Element Poloroid Filter Paper & Ground Glass Diffuser Installed Between Backlite & Window
-107	.020	MMH	300	1.6	Amb	Amb	100	0.330	1350	385	385	10/7/74	8	400	Normal	15	Long Impingement Element
-108	.020	MMH	250	1.6	Amb	Amb	100	0.330	1095	335	335	10/7/74	8	400	Normal	15	Long Impingement Element
-109	.020	MMH	200	1.6	Amb	Amb	100	0.432	1568	285	285	10/7/74	8	400	Normal	15	Long Impingement Element
-110	.020	MMH	150	1.6	Amb	Amb	100	0.432	1129	235	235	10/7/74	8	400	Normal	15	Long Impingement Element
-111	.020	MMH	100	1.6	Amb	Amb	100	0.563	1350	185	185	10/7/74	3.3	8000	Normal	15	Long Impingement Element
-112	.020	A-50	100	1.6	Amb	Amb	20	0.563	1533	105	105	10/8/74	3.3	8000	1 Stop	15	Long Impingement Element Moved camera to opposite Window & added front lighting
-113	.020	A-50	100	1.6	Amb	Amb	100	0.563	1350	185	185	10/12/74	5.6	400	Normal	14	Long Impingement Element

Table IV

Test No.	D_f	Fuel	P_c	MR	T_F	T_o	ΔP_f	Noz	P_{N2} (PSIG)	P_{OT} (PSIG)	P_{FT} (PSIG)	DATE	f-Stop	FR/Rate (PPS)	Process	Light Meter W/2 N.D.F.	REMARKS
OC-27-114	.020	A-50	150	1.6	Amb	Amb	100	0.432	1129	235	235	10/12/74	5.6	400	Normal	14	Long Impingement Element
-115	.020	A-50	200	1.6	Amb	Amb	100	0.432	1568	285	285	10/12/74	5.6	400	Normal	14	Long Impingement Element
-116	.020	A-50	250	1.6	Amb	Amb	100	0.330	1095	335	335	10/12/74	5.6	400	Normal	14	Long Impingement Element
-117	.020	A-50	300	1.6	Amb	Amb	20	0.330	1646	305	305	10/12/74	5.6	400	Normal	14	Long Impingement Element
-118	.020	A-50	300	1.6	Amb	Amb	100	0.330	1350	385	385	10/12/74	5.6	400	Normal	14	Long Impingement Element
-119	.020	A-50	500	1.6	Amb	Amb	100	0.265	1463	585	585	10/12/74	5.6	400	Normal	14	Long Impingement Element
-120	.020	A-50	1000	1.6	Amb	Amb	100	0.187	1463	1085	1085	10/12/74	5.6	400	Normal	14	Long Impingement Element
-121	.020	A-50	150	1.6	Amb	Amb	100	0.432	1129	235	235	10/12/74	5.6	400	Normal	14	Rerun of #114 Reduced window purge from 10X to 1X
-122	.020	A-50	300	1.6	Amb	Amb	100	0.187	360	385	385	10/12/74	3.3	4000	Normal	14	Long Impingement Element
-123	.020	A-50	300	1.6	Amb	Amb	100	0.187	360	385	385	10/12/74	3.3	4000	Normal	14	Repeat of 122
-124	.020	MMH	1000	1.6	Amb	Amb	100	0.187	1463	1085	1085	10/16/74	5.6	400	Push 1 Stop	14	Increased purge flow to 10X Short Impingement Element
-125	.020	MMH	500	1.6	Amb	Amb	100	0.265	1463	585	585	10/16/74	5.6	400	Push 1 Stop	14	Short Impingement Element
-126	.020	MMH	300	1.6	Amb	Amb	100	0.330	1350	385	385	10/16/74	5.6	400	Push 1 Stop	14	Short Impingement Element
-127	.020	MMH	300	1.6	Amb	Amb	20	0.330	1646	305	305	10/16/74	5.6	400	Push 1 Stop	14	Short Impingement Element
-128	.020	MMH	250	1.6	Amb	Amb	100	0.330	1095	335	335	10/16/74	5.6	400	Push 1 Stop	14	Short Impingement Element
-129	.020	MMH	200	1.6	Amb	Amb	100	0.432	1568	285	285	10/16/74	5.6	400	Push 1 Stop	14	Short Impingement Element
-130	.020	MMH	150	1.6	Amb	Amb	100	0.432	1129	235	235	10/16/74	5.6	400	Push 1 Stop	14	Short Impingement Element

Table IV

Test No.	D_f	Fuel	P_c	R	T_F	T_o	ΔP_f	Noz	P_{N2} (PSIG)	P_{OT} (PSIG)	P_{FT} (PSIG)	DATE	f-Stop	FR/Rate (PPS)	Process	W/2 N.D.F.	REMARKS
OC-27-131	.020	MMH	100	1.6	Amb	Amb	100	0.563	1350	185	185	10/16/74	5.6	400	Push 1 Stop	14	Short Impingement Element
-132	.020	MMH	125	1.6	Amb	Amb	100	0.563	1732	210	210	10/16/74	3.3	4000	Push 1 Stop	14	Short Impingement Element
-133	.020	MMH	500	1.6	Amb	Amb	100	0.265	1463	585	585	10/17/74	Still Photo				Long Impingement Element
-134	.020	MMH	100	1.6	200	Amb	100	0.563	1350	185	185	10/23/74	5.6	400	Push 1 Stop	14	Long Impingement Element
-135	.020	MMH	125	1.6	200	Amb	100	0.563	1923	210	210	10/23/74	5.6	400	Push 1 Stop	14	Long Impingement Element
-136	.020	MMH	150	1.6	200	Amb	100	0.432	1129	235	235	10/23/74	5.6	400	Push 1 Stop	14	Long Impingement Element
-137	.020	MMH	200	1.6	200	Amb	100	0.432	1568	285	285	10/23/74	5.6	400	Push 1 Stop	14	Long Impingement Element
-138	.020	MMH	250	1.6	200	Amb	100	0.330	1095	335	335	10/23/74	5.6	400	Push 1 Stop	14	Long Impingement Element Heater Pump Seal Malf. installed T/C @ Imping. Pt.
-139	.020	MMH	100	1.6	Amb	Amb	20	0.563	2110	101	105	10/25/74	5.6	400	Push 1 Stop	14	Long Impingement Element
-140	.020	MMH	100	1.6	Amb	Amb	100	0.563	1350	181	185	10/25/74	5.6	400	Push 1 Stop	14	
-141	.020	MMH	100	1.6	Amb	Amb	100	0.563	1350	181	185	10/25/74	5.6	400	Push 1 Stop	14	Changed T/C from 0.01" Dia. to 0.02" Dia. prior to test 142
-142	.020	MMH	125	1.6	Amb	Amb	100	0.563	1923	206	210	10/25/74	5.6	400	Push 1 Stop	14	Long Impingement Element
-143	.020	MMH	125	1.6	Amb	Amb	20	0.432	1516	126	130	10/25/74	5.6	400	Push 1 Stop	14	Long Impingement Element
-144	.020	MMH	150	1.6	Amb	Amb	20	0.432	1839	151	155	10/25/74	5.6	400	Push 1 Stop	14	Long Impingement Element
-145	.020	MMH	150	1.6	Amb	Amb	100	0.432	1129	231	235	10/25/74	5.6	400	Push 1 Stop	14	Long Impingement Element
-145	.020	MMH	200	1.6	Amb	Amb	100	0.432	1568	281	285	10/25/74	5.6	400	Push 1 Stop	14	Long Impingement Element

TABLE IV

Test No.	D_f	Fuel	P_c	MR	T_F	T_o	ΔP_f	Ncz	(PSIG)	(PSIG)	(PSIG)	DATE	f-Stop	FR/Rate (PPS)	Process	W/Z N.D.F.	REMARKS
OC-27-147	.020	MMH	250	1.6	Amb	Amb	100	0.330	1095	331	335	10/25/74	5.6	400	Push 1 Stop	14	Long Impingement Element
-148	.020	MMH	100	1.6	Amb	Amb	20	0.563	2110	101	105	10/25/74	5.6	400	Push 1 Stop	14	Long Impingement Element
-149	.020	MMH	100	1.6	Amb	Amb	100	0.563	1350	181	185	10/25/74	5.6	400	Push 1 Stop	14	Long Impingement Element
-150	.020	MMH	300	1.6	Amb	Amb	100	0.330	1350	381	385	10/25/74	5.6	400	Push 1 Stop	14	Long Impingement Element
-151	.020	MMH	500	1.6	Amb	Amb	100	0.265	1463	581	585	10/25/74	5.6	400	Push 1 Stop	14	Long Impingement Element
-152	.020	MMH	1000	1.6	Amb	Amb	100	0.187	1463	1081	1085	10/25/74	5.6	400	Push 1 Stop	14	Long Impingement Element

ORIGINAL PAGE IS OF POOR QUALITY

TABLE V - COMPUTER LISTING - TEST SUMMARY

HIGH PERFORMANCE N2O4 / AMINE ELEMENTS

HYPERGOLIC STREAM IMPINGMENT DATA COMPLIATION

INVESTIGATOR LAWVER

A L R C MODEL CORRELATION PARAMETERS

FUEL TYPE	TEST NO.	DO (IN)	DF (IN)	L/D	IMP ANGLE (DEG)	PC (PSIA)	VO (FT/S)	VF (FT/S)	TO (F)	TF (F)	MR	MF/MO	COMMENTS	*	DIV (SEC)	FNF (LBF)	DNF (PSIA)
MMH	101	.022	.020	24.	60.	308.	107.6	129.1	88.	87.	1.66	.875	SEP	*	.31-03	.00	.00
MMH	102	.022	.020	24.	60.	308.	104.7	132.5	88.	87.	1.57	.975	SEP	*	.30-03	.00	.00
MMH	103	.022	.020	24.	60.	309.	106.4	129.9	88.	87.	1.62	.908	SEP	*	.31-03	.00	.00
MMH	104	.022	.020	24.	60.	311.	105.1	129.1	88.	87.	1.62	.918	SEP	*	.31-03	.00	.00
MMH	105	.022	.020	24.	60.	507.	107.7	125.7	89.	88.	1.70	.829	SEP	*	.32-03	.00	.00
MMH	106	.022	.020	24.	60.	1000.	109.5	138.5	89.	88.	1.57	.975	SEP	*	.29-03	.00	.00
MMH	107	.022	.020	24.	60.	308.	106.6	124.7	86.	85.	1.70	.832	SEP	*	.32-03	.00	.00
MMH	108	.022	.020	24.	60.	263.	103.0	124.6	84.	84.	1.65	.889	SEP	*	.32-03	.00	.00
MMH	109	.022	.020	24.	60.	197.	112.8	136.5	84.	84.	1.64	.889	SEP	*	.29-03	.00	.00
MMH	110	.022	.020	24.	60.	158.	104.6	129.6	83.	83.	1.60	.932	SEP	*	.31-03	.00	.00
MMH	111	.022	.020	24.	60.	100.	109.8	135.5	84.	83.	1.60	.926	MIX	*	.29-03	.00	.00
A-50	112	.022	.020	24.	60.	89.	60.9	76.3	76.	76.	1.59	.954	MIX	*	.52-03	.00	.00
A-50	113	.022	.020	24.	60.	101.	108.9	132.5	88.	87.	1.63	.900	MIX	*	.30-03	.00	.00
A-50	114	.022	.020	24.	60.	162.	101.6	121.9	82.	82.	1.66	.875	MIX	*	.33-03	.00	.00
A-50	115	.022	.020	24.	60.	203.	108.3	130.1	81.	78.	1.65	.878	SEP	*	.31-03	.00	.00
A-50	116	.022	.020	24.	60.	269.	99.3	118.2	80.	77.	1.67	.862	SEP	*	.34-03	.00	.00
A-50	117	.022	.020	24.	60.	301.	73.3	88.6	78.	76.	1.64	.888	SEP	*	.45-03	.00	.00
A-50	118	.022	.020	24.	60.	310.	103.2	127.8	81.	81.	1.60	.931	SEP	*	.31-03	.00	.00
A-50	119	.022	.020	24.	60.	510.	102.0	124.4	82.	82.	1.64	.904	SEP	*	.32-03	.00	.00
A-50	120	.022	.020	24.	60.	1003.	104.5	126.9	82.	81.	1.63	.896	SEP	*	.31-03	.00	.00
A-50	121	.022	.020	24.	60.	160.	105.7	129.4	81.	80.	1.62	.910	MIX	*	.31-03	.00	.00
A-50	122	.022	.020	24.	60.	338.	86.6	104.0	81.	80.	1.65	.876	SEP	*	.38-03	.00	.00
A-50	123	.022	.020	24.	60.	334.	89.7	108.0	77.	77.	1.65	.880	SEP	*	.37-03	.00	.00
MMH	124	.022	.020	24.	60.	955.	82.9	101.6	82.	82.	1.61	.913	SEP	*	.39-03	.00	.00
MMH	125	.022	.020	24.	60.	495.	105.5	130.3	83.	81.	1.60	.928	SEP	*	.31-03	.00	.00
MMH	126	.022	.020	24.	60.	298.	105.5	132.1	83.	82.	1.59	.953	SEP	*	.30-03	.00	.00
MMH	127	.022	.020	24.	60.	283.	63.9	80.5	84.	81.	1.58	.969	SEP	*	.49-03	.00	.00
MMH	128	.022	.020	24.	60.	256.	101.0	126.2	85.	83.	1.58	.951	SEP	*	.32-03	.00	.00
MMH	129	.022	.020	24.	60.	191.	109.1	135.5	85.	83.	1.60	.940	SEP	*	.29-03	.00	.00
MMH	130	.022	.020	24.	60.	152.	102.2	129.5	85.	82.	1.56	.977	SEP	*	.31-03	.00	.00
MMH	131	.022	.020	24.	60.	95.	105.7	133.0	85.	83.	1.57	.964	MIX	*	.30-03	.00	.00
MMH	132	.022	.020	24.	60.	114.	108.7	136.4	86.	83.	1.58	.958	MIX	*	.29-03	.00	.00
MMH	133	.022	.020	24.	60.	411.	149.7	179.6	83.	83.	1.66	.874	SEP	*	.22-03	.00	.00
MMH	134	.022	.020	24.	60.	97.	110.4	136.3	77.	197.	1.74	.859	SEP	*	.29-03	.00	.00
MMH	135	.022	.020	24.	60.	119.	111.8	139.2	78.	199.	1.72	.873	SEP	*	.29-03	.00	.00
MMH	136	.022	.020	24.	60.	150.	110.0	136.5	77.	199.	1.74	.866	SEP	*	.29-03	.00	.00
MMH	137	.022	.020	24.	60.	188.	116.2	143.6	76.	199.	1.74	.860	SEP	*	.28-03	.00	.00
MMH	138	.022	.020	24.	60.	243.	111.0	148.9	79.	195.	1.60	1.015	SEP	*	.27-03	.00	.00
MMH	139	.022	.020	24.	60.	103.	42.5	58.4	61.	59.	1.45	1.140	UNDEF	*	.68-03	.00	.00
MMH	140	.022	.020	24.	60.	81.	115.9	143.0	64.	62.	1.61	.922	UNDEF	*	.26-03	.00	.00

HIGH PERFORMANCE N_2O_4 / AMINE ELEMENTS

HYPERGOLIC STREAM IMPINGMENT DATA COMPLIATION

INVESTIGATOR LAWVER

A L R C MODEL CORRELATION PARAMETERS

FUEL TYPE	TEST NO.	DO (IN)	DF (IN)	L/D	IMP ANGLE (DEG)	PC (PSIA)	VO (FT/S)	VF (FT/S)	TO (F)	TF (F)	MR	MF/MO	COMMENTS	*	DIV (SEC)	FNF (LBF)	DNF (PSIA)
MMH	141	.022	.020	24.	60.	81.	115.2	143.2	66.	64.	1.60	.935	UNDEF	*	.28-03	.00	.00
MMH	142	.022	.020	24.	60.	119.	108.7	136.7	68.	67.	1.59	.958	MIX	*	.29-03	.00	.00
MMH	143	.022	.020	24.	60.	129.	38.6	54.2	67.	67.	1.42	1.193	UNDEF	*	.73-03	.00	.00
MMH	144	.022	.020	24.	60.	154.	42.8	55.7	67.	67.	1.53	1.026	UNDEF	*	.71-03	.00	.00
MMH	145	.022	.020	24.	60.	152.	104.9	128.4	66.	67.	1.62	.906	SEP	*	.31-03	.00	.00
MMH	146	.022	.020	24.	60.	190.	107.5	135.9	68.	67.	1.57	.968	SEP	*	.29-03	.00	.00
MMH	147	.022	.020	24.	60.	258.	100.7	124.2	66.	67.	1.61	.920	SEP	*	.32-03	.00	.00
MMH	148	.022	.020	24.	60.	102.	44.1	58.8	66.	68.	1.49	1.075	MIX	*	.68-03	.00	.00
MMH	149	.022	.020	24.	60.	99.	106.7	133.6	69.	69.	1.60	.948	MIX	*	.30-03	.00	.00
MMH	150	.022	.020	24.	60.	297.	107.2	131.9	70.	69.	1.62	.916	SEP	*	.30-03	.00	.00
MMH	151	.022	.020	24.	60.	484.	113.5	137.8	70.	69.	1.64	.892	SEP	*	.29-03	.00	.00
MMH	152	.022	.020	24.	60.	958.	121.1	146.3	78.	74.	1.62	.912	SEP	*	.27-03	.00	.00

OPENING FILE 1RSS$142152 FOR PLOTTING

ZETA PLOT FILE 1RSS$142152 CONTAINS 59 LINES

GFIN

TABLE VI

HIGH PRESSURE RSS LIMITS

Fuel	Predicted Limit	Measured Limit
N_2H_4	300	300
MMH	400	150
A-50	500	200

TABLE VII

COMPARISON OF HEAT RELEASE RATES AND RSS LIMIT

Fuel	P_V (psia) at 100°F	Heat Release Rate Kcal/sec-mole of NTO	Sep. Limit
N_2H_4	0.65	4×10^4	300
A-50	4.6	-	200
UDMH	11.0	14×10^4	-
MMH	2.1	20×10^4	150

TABLE VIII

HIGH FREQUENCY RESPONSE INSTRUMENTATION

Test Parameter	Symbol	Instrument Make	Model	Range	Accuracy
Oxidizer Manifold Pressure	POJHF	Kistler	601	0-3000 psi (P-P)	± 0.5%
Fuel Manifold Pressure	PFJHF	Kistler	601	0-3000 psi (P-P)	± 0.5%
Chamber Pressure	PCHF	Kistler	601	0-3000 psi (P-P)	± 0.5%
Injector Acceleration	ACC	-	-	0-500 g's	± 0.5%
Injector Probe Temperature	TP1	C/A		0-500 °F	± 1%

TABLE IX

LOW FREQUENCY RESPONSE INSTRUMENTATION

TEST PARAMETER	SYMBOL	RANGE	UNITS	RECORDER "O" GRAPH	RECORDER TAPE	RECORDER DIGITAL
Oxid. Tank Pressure	POT	0-1500	PSIA	X		
Fuel Tank Pressure	PFT	0-1500	PSIA	X		
Oxid. Injector Pressure	POJ	0-1500	PSIA	X		X
Fuel Injector Pressure	PFJ	0-1500	PSIA	X		X
Chamber Pressure	PC	0-1000	PSIA	X		X
Window Purge Pressure	PNZ	0-2000	PSIA	X		X
Oxid. Flowrate	WO	0-0.1	LB/SEC	X		X
Fuel Flowrate	WF	0-0.1	LB/SEC	X		X
Oxid. Flowmeter Temp.	TOFM	0-500	^oF	X		X
Fuel Flowmeter Temp.	TFFM	0-500	^oF	X		X
Oxid. Injector Temp.	TOJ	0-500	^oF	X		
Fuel Injector Temp.	TFJ	0-500	^oF	X		
Oxid. Valve Voltage	VOV			X		
Fuel Valve Voltage	VFW			X		
Wind Purge Valve Voltage	VWPV			X		
Camera Voltage	VCAM			X	X	
Injector Purge Valve Voltage	VIPV			X		

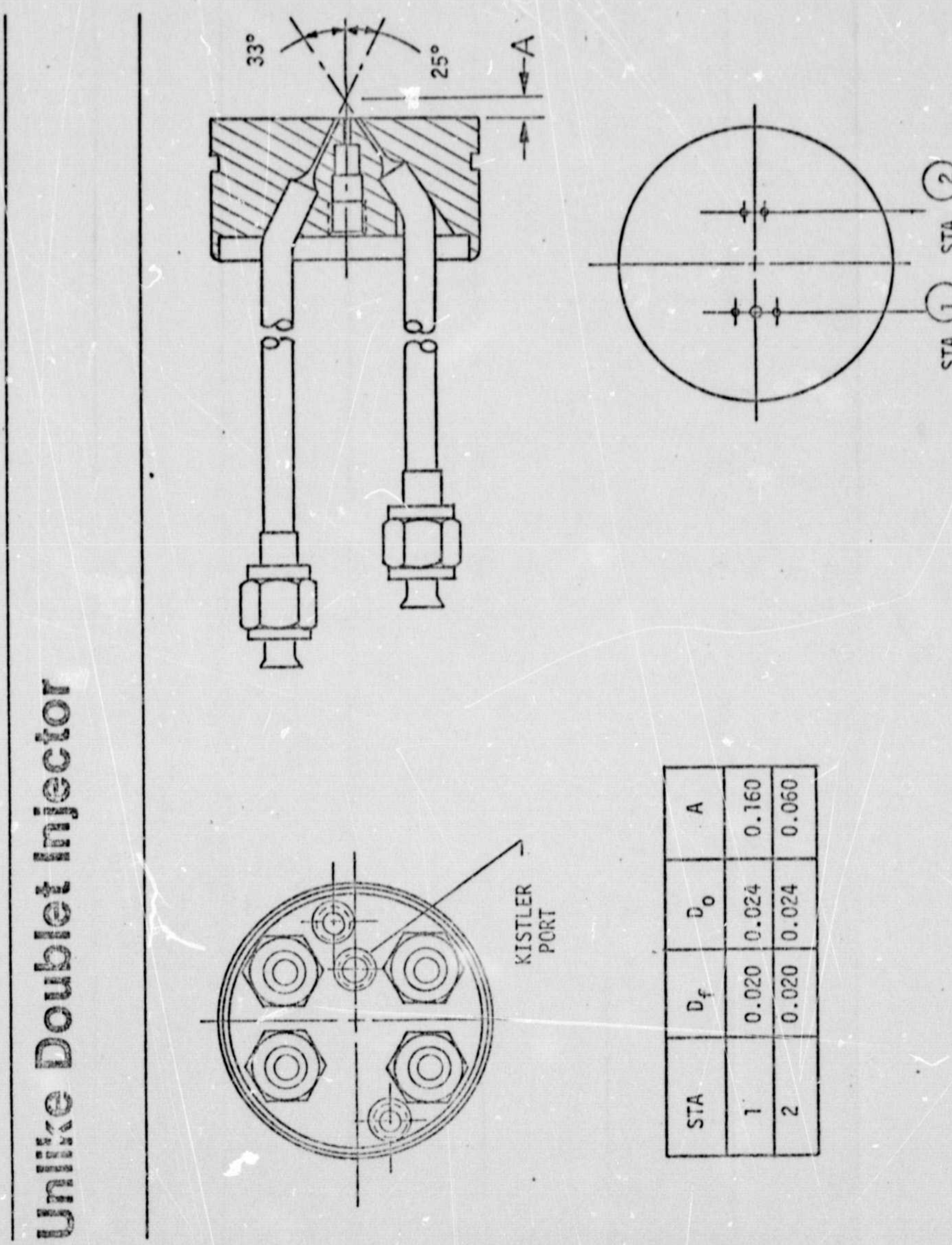

STA	D_f	D_o	A
1	0.020	0.024	0.160
2	0.020	0.024	0.060

FIGURE 1. UNLIKE DOUBLET INJECTOR

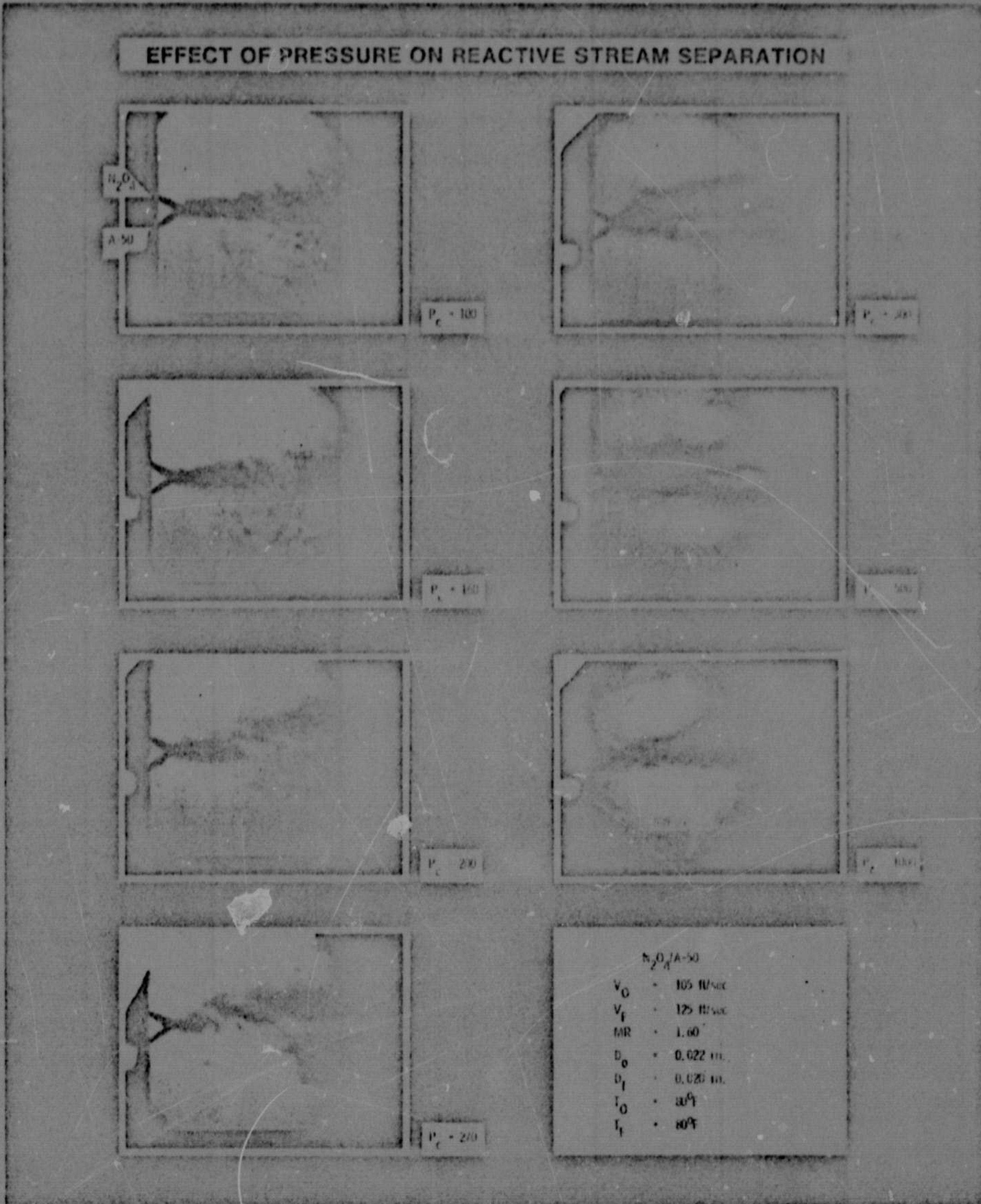

FIGURE 2. EFFECT OF PRESSURE ON REACTIVE STREAM SEPARATION

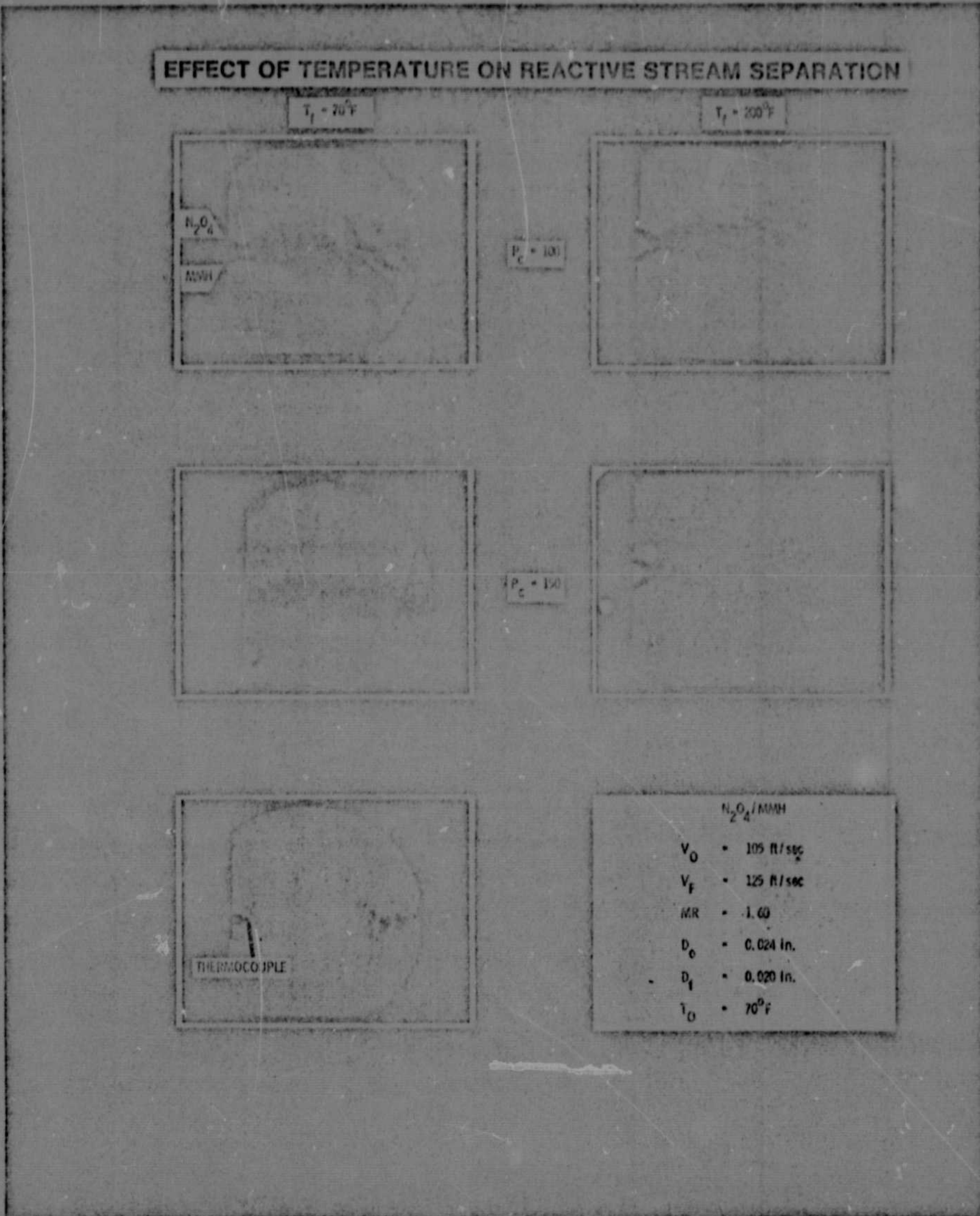
EFFECT OF TEMPERATURE ON REACTIVE STREAM SEPARATION
T_f = 70°F
T_f = 200°F
N_2O_4
MMH
P_c = 100
P_c = 150
THERMOCOUPLE
N_2O_4/MMH
V_O = 105 ft/sec
V_F = 125 ft/sec
MR = 1.60
D_o = 0.024 in.
D_f = 0.020 in.
T_O = 70°F

FIGURE 3.

FIG 4. EFFECT OF PRESSURE AND VELOCITY ON IMPINGEMENT POINT TEMPERATURE

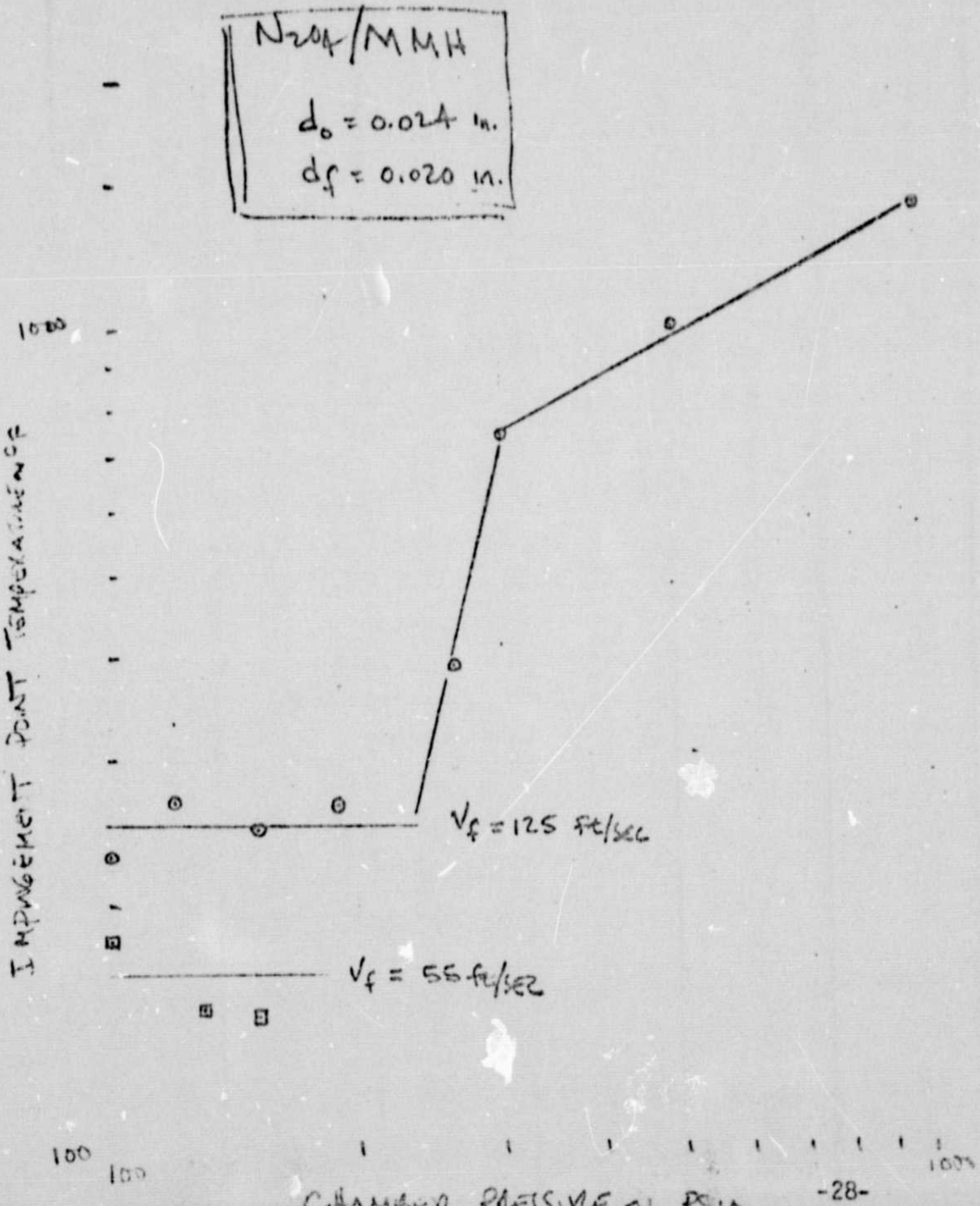

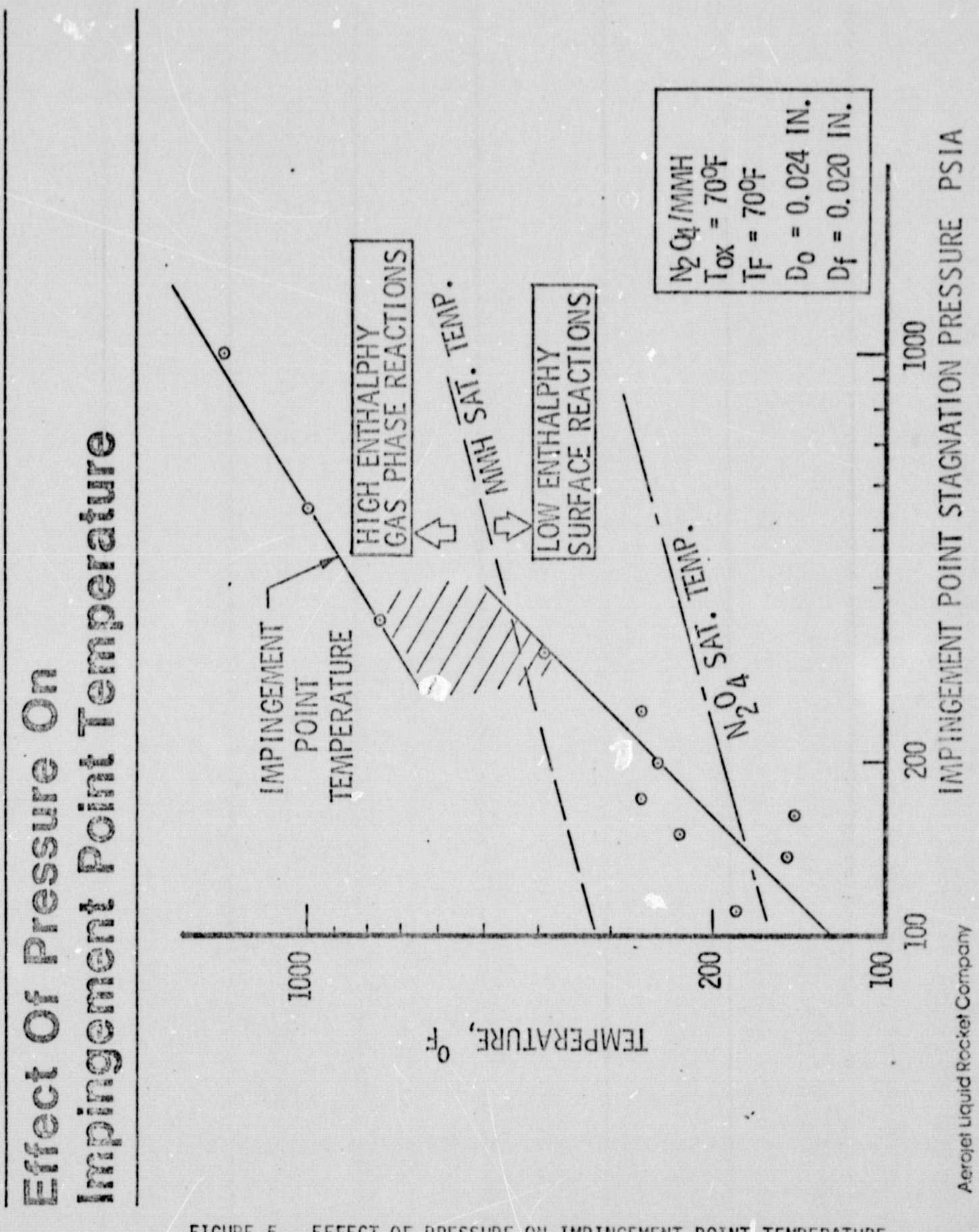

FIGURE 5. EFFECT OF PRESSURE ON IMPINGEMENT POINT TEMPERATURE

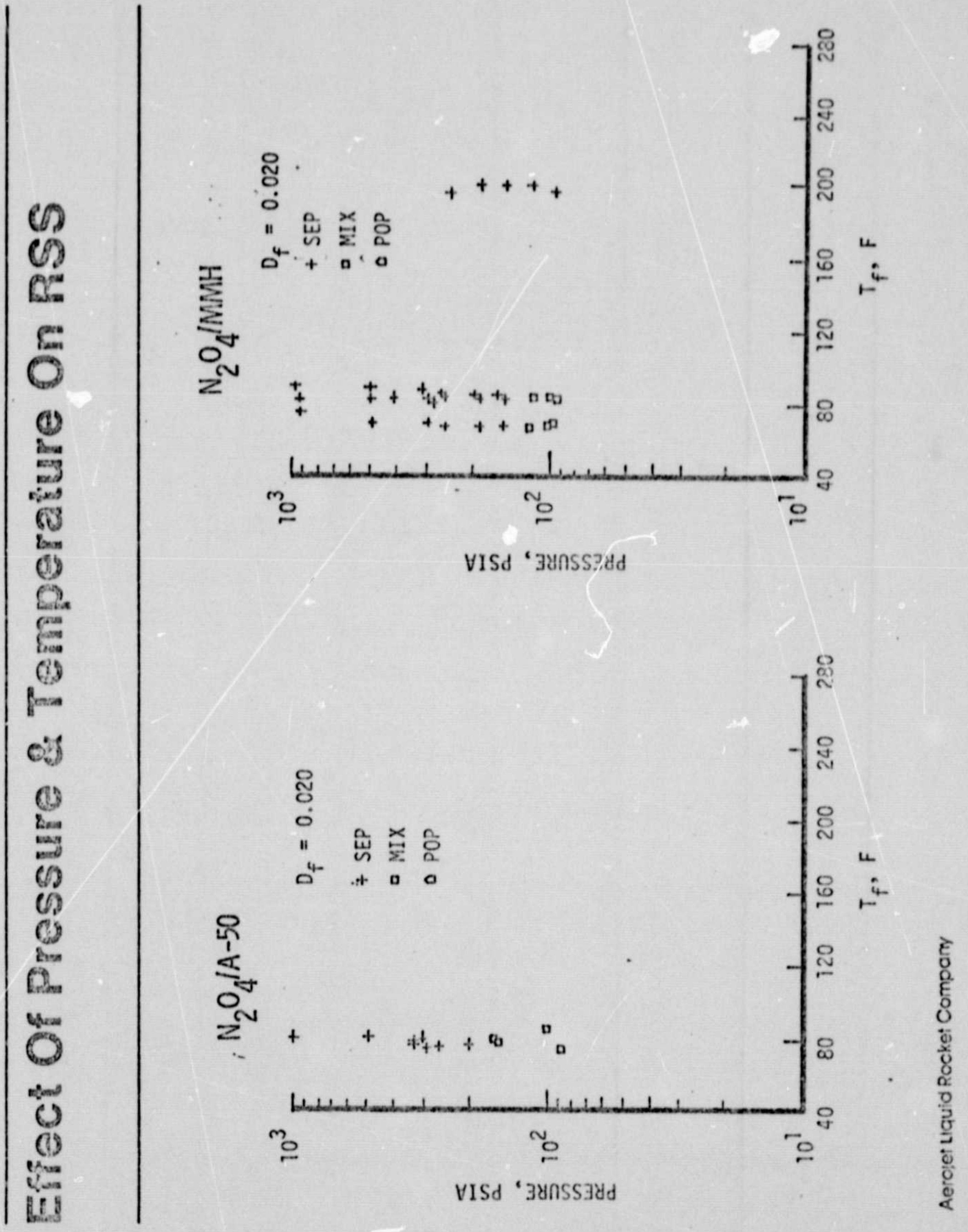

FIGURE 6. EFFECT OF PRESSURE AND TEMPERATURE ON RSS

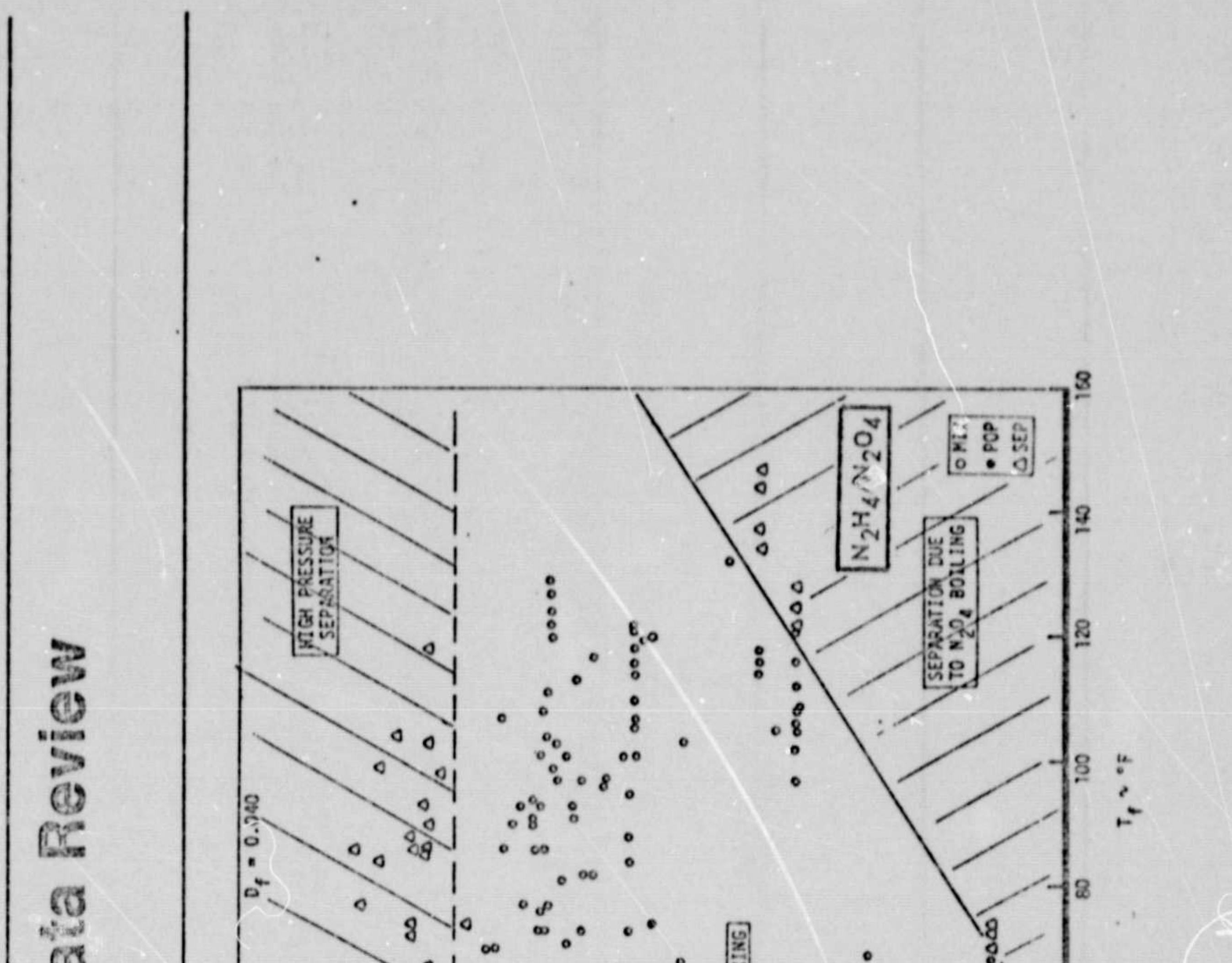

FIGURE 7. TASK I - DATA PLOT

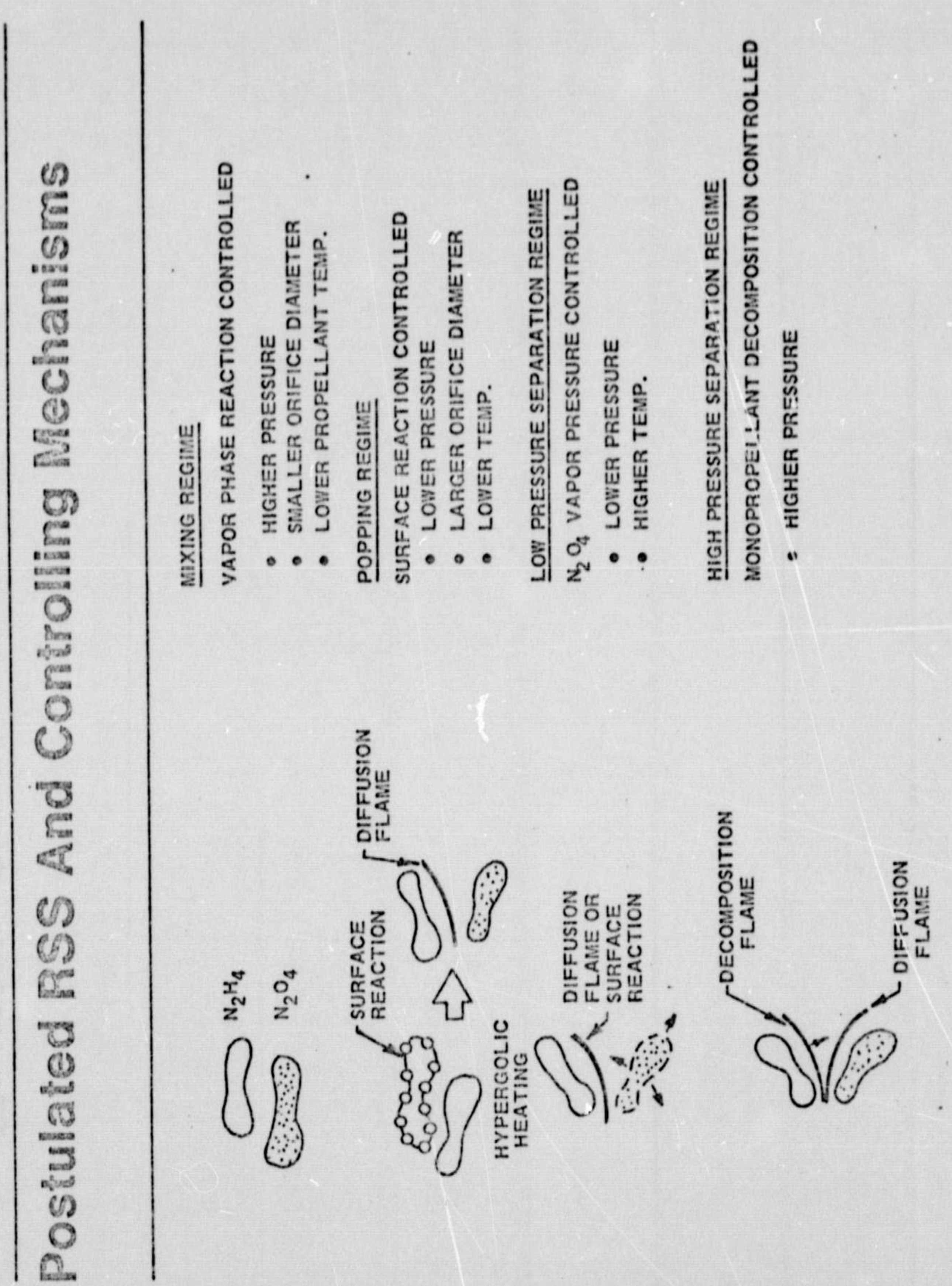

FIGURE 8. POSTULATED RSS AND CONTROLLING MECHANISMS

FIG. 9 - EFFECT OF REYNOLDS NO. ON IMPINGEMENT POINT TEMPERATURE RISE

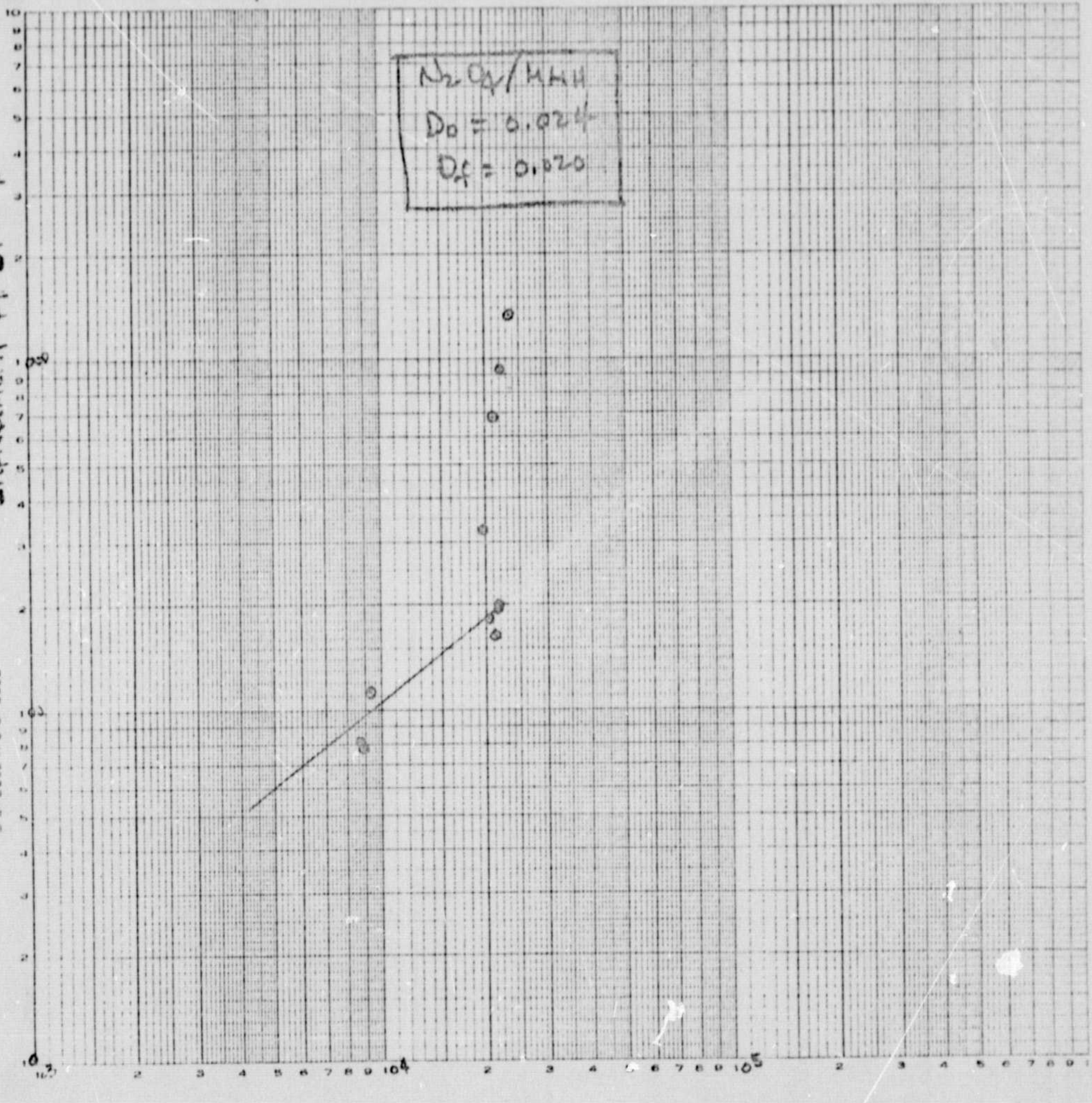

Fig. 10 - EFFECT OF WEBER No. ON IMPINGEMENT PT. TEMPERATURE BASE

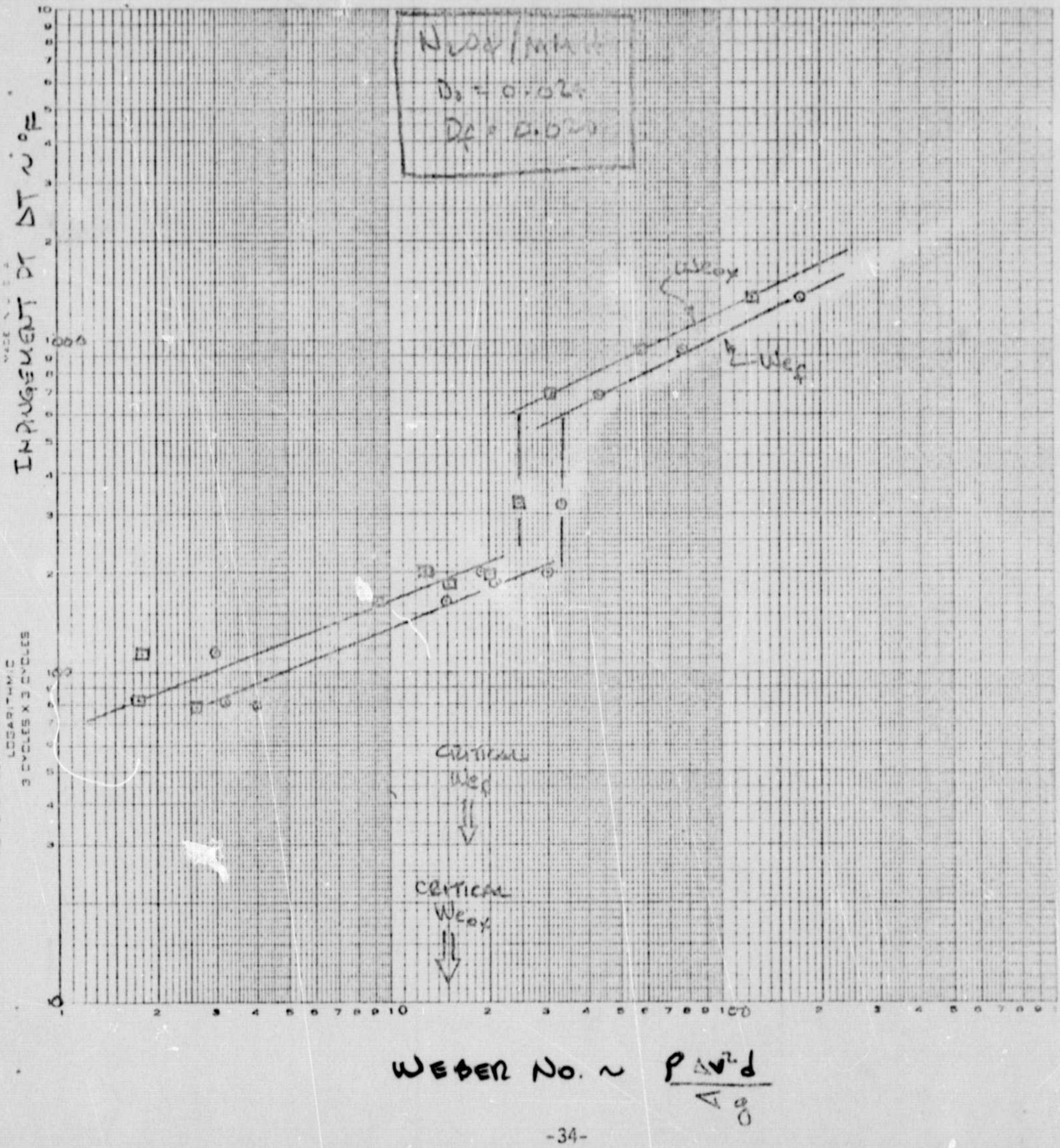

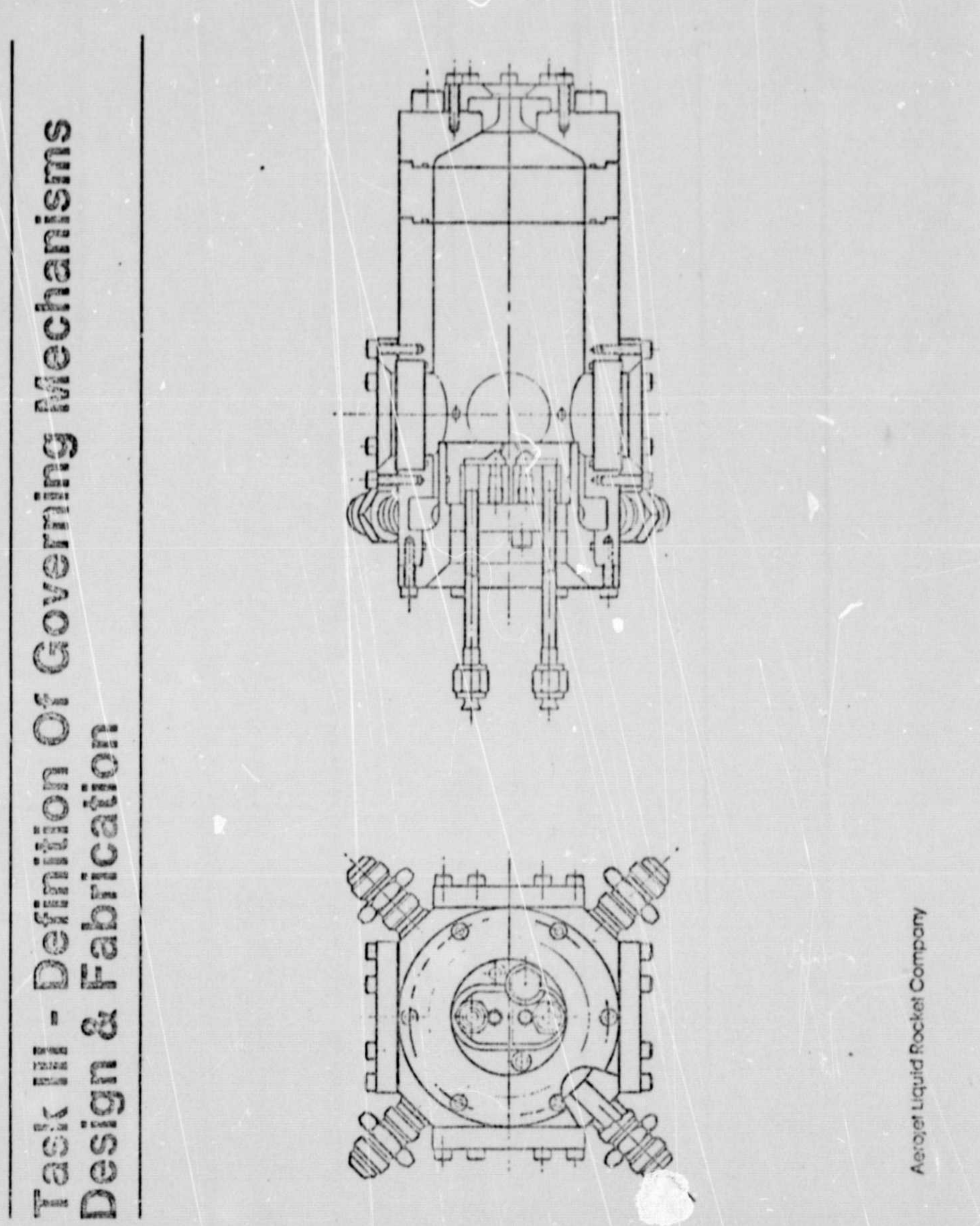

FIGURE 11. TASK III - TEST CHAMBER

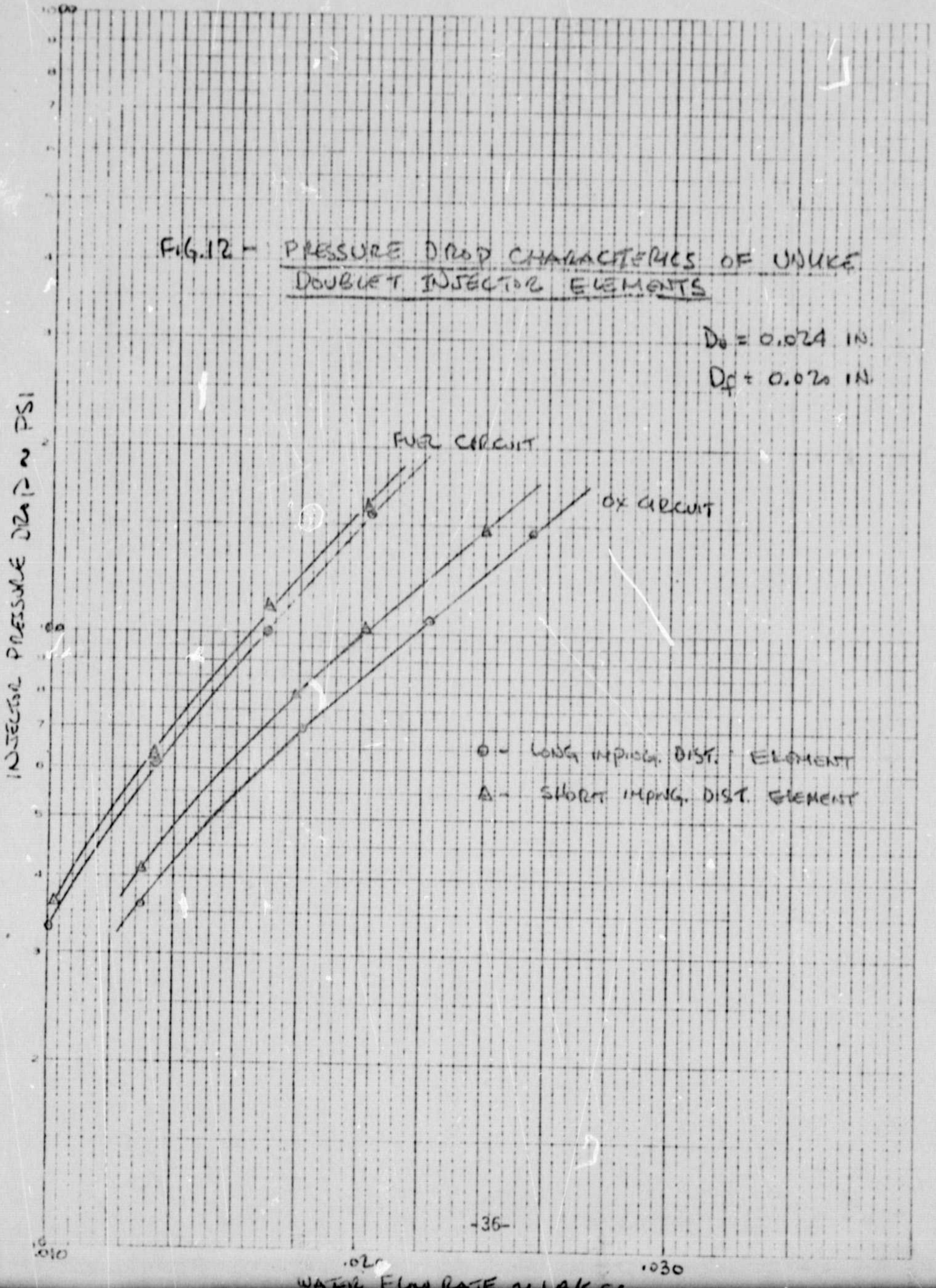

FIG.12 - PRESSURE DROP CHARACTERISTICS OF UNLIKE DOUBLET INJECTOR ELEMENTS

Task III - Definition Of Governing Mechanisms Photographic Setup

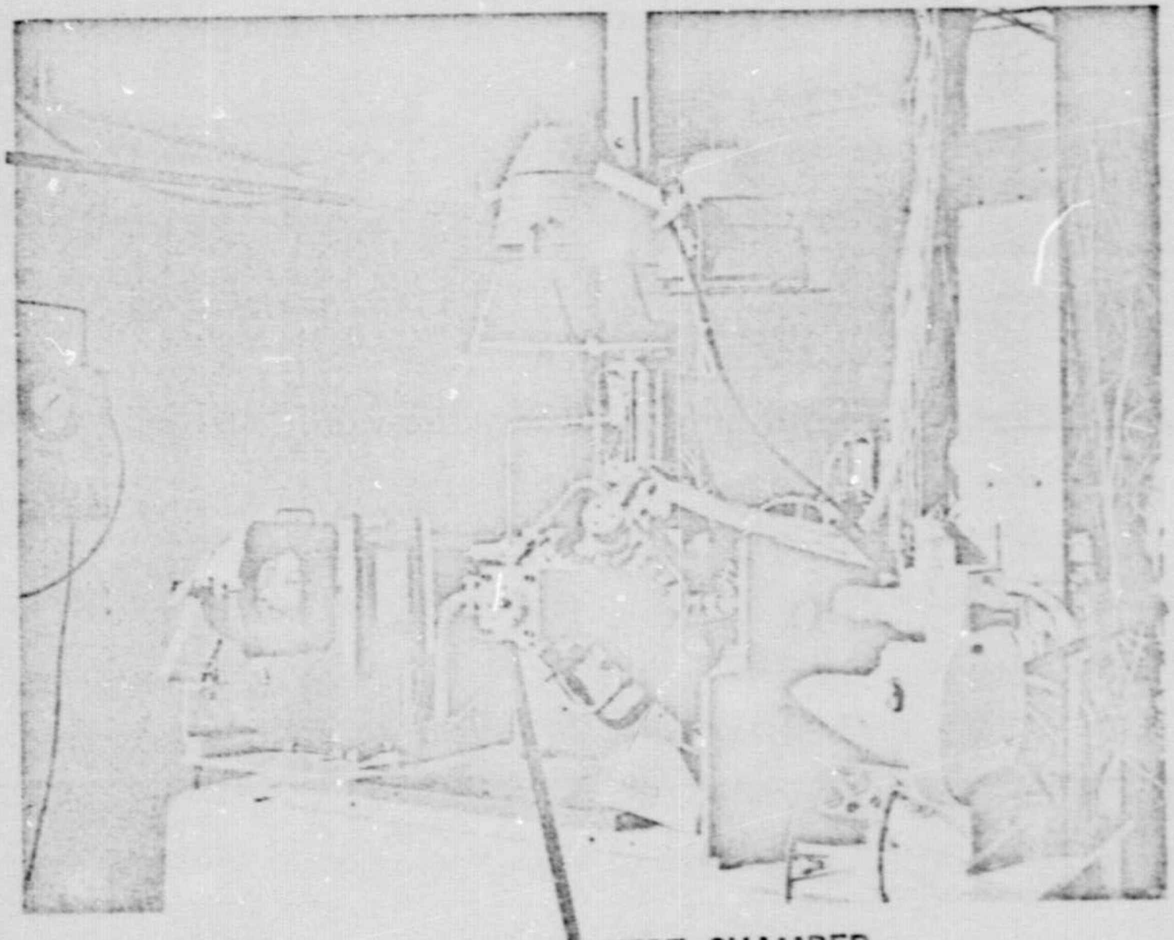

FIGURE 13. TASK III - PHOTOGRAPHIC SETUP

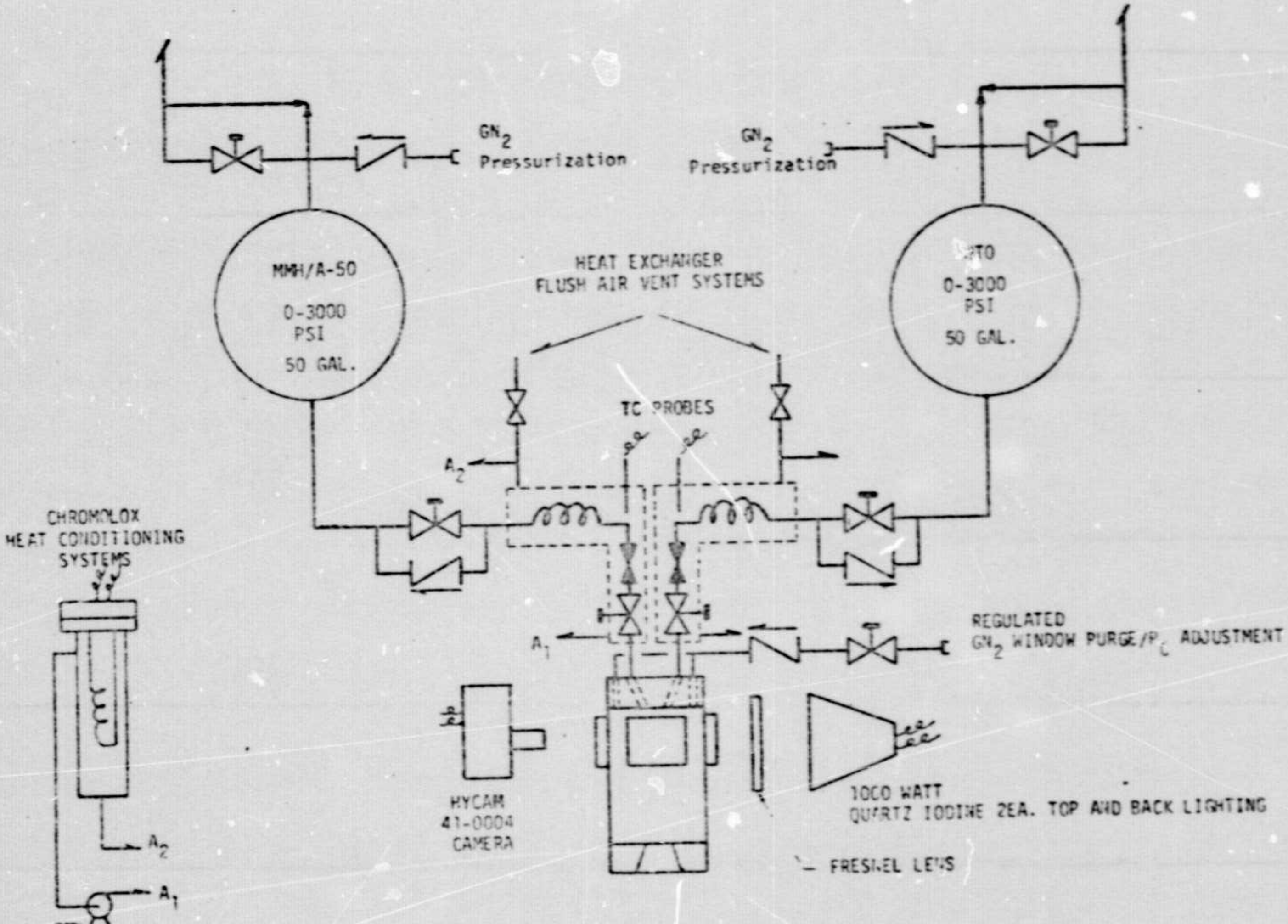

Figure 14. Propellant Flow System Schematic

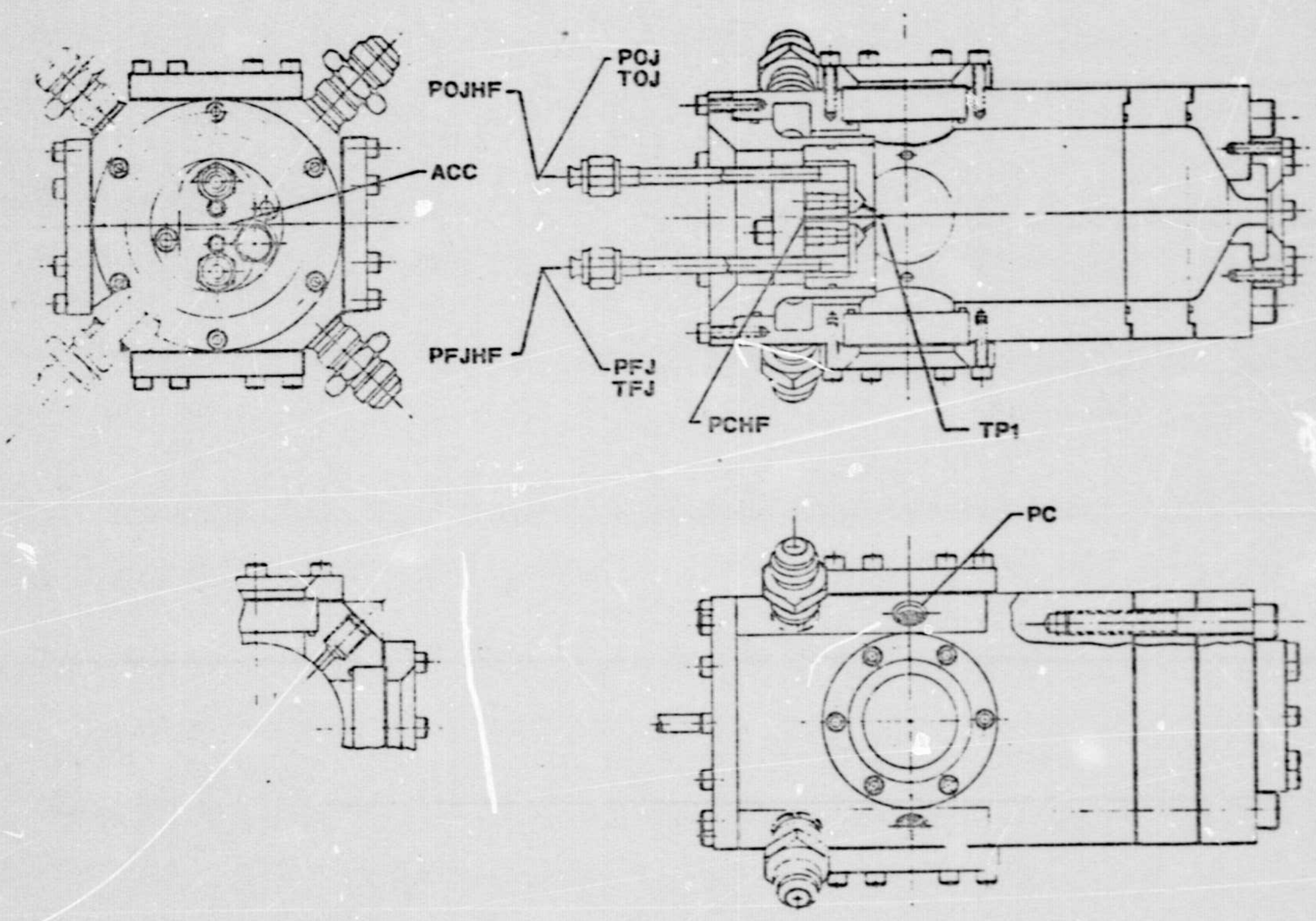

Figure 15. Instrumentation Schematic